

Supporting Information for

Understanding How Acoustic Vibrations Modulate

the Optical Response of Plasmonic Metal

Nanoparticles

*Aftab Ahmed <sup>§,‡,\*</sup>, Matthew Pelton <sup>†,‡</sup>, Jeffrey R. Guest <sup>‡,\*</sup>*

<sup>§</sup> Department of Electrical Engineering, California State University Long Beach, CA 90840,  
United States

<sup>†</sup> Department of Physics, University of Maryland, Baltimore County, MD 21250, United States

<sup>‡</sup> Center for Nanoscale Materials, Argonne National Laboratory, Argonne, Illinois 60439, United  
States

## PERMITTIVITY OF THE DEFORMED NANOPARTICLE

The dielectric response of a metal can be modeled using the Lorentz-Drude model:

$$\varepsilon_r(\omega) = \varepsilon_r(\infty) + \omega_p^2 \sum_{m=0}^M \frac{f_m}{\omega_{0,m}^2 - \omega^2 - j\omega\Gamma_m}, \quad (\text{S1})$$

where  $\omega_p$  is the bulk plasma frequency,  $f_m$  is the oscillator strength of the  $m^{\text{th}}$  Lorentzian term,  $\omega_{0,m}$  are the inter-band transition frequencies, and  $\Gamma_m$  is the linewidth. These parameters are obtained for gold and silver by fitting Equation S1 to the experimental data of Refs. [1,2], providing the relative permittivity of a non-deformed nanoparticle. The fitted parameters are given in Table 1; the Drude part of the response is obtained by setting  $\omega_{0,0} = 0$ .

As the volume of the particle changes, the free electron density increases or decreases. The free-electron density,  $N$ , of a deformed nanoparticle is  $N = N_0/(1 + \Delta V/V_0)$ , where  $N_0$  and  $V_0$  are the free electron density and volume of the non-deformed nanoparticle, respectively, and  $\Delta V$  is the change in volume as the particle deforms. The change in volume is calculated for each nanoparticle geometry and each vibrational mode from the mode shapes given by finite-element (FE) calculations. Changes in free electron density affect the bulk plasma frequency  $\omega_p = \sqrt{(Ne^2)/(\varepsilon_0 m)}$ , where  $e$  and  $m$  are the charge and effective mass of the electron, respectively, and  $\varepsilon_0$  is the free space permittivity. The change in  $\omega_p$ , in turn, modifies the relative permittivity in accordance with Equation S1.

The inter-band transition frequencies  $\omega_{0,m}$  are also modified as the particle undergoes compression or expansion. The shifts in  $\omega_{0,m}$  are calculated using the deformation potentials (DP) for gold and silver:  $\delta E_{0,m} = \xi_m (dV/V)$ , where  $\xi_m$  and  $\delta E_{0,m}$  are the DPs and change in energy of the  $m^{\text{th}}$  transition,<sup>3-4</sup> and the local dilations are

$$\frac{dV}{V} = e_{xx} + e_{yy} + e_{zz} , \quad (\text{S2})$$

where  $e_{ij}$  are the local strains. Because deformations are small, we can neglect  $e_{ij}$  for  $i \neq j$ . The inset in Figure S1b shows, as an example, the local dilation within a gold nanosphere corresponding to the fundamental breathing mode of the sphere.

**Table 1.** Parameters used to model the optical response of gold and silver.

Parameter	Gold	Silver
$\omega_p$	$13.716 \times 10^{15}$ (rad/s)	$1.368 \times 10^{16}$ (rad/s)
$\Gamma_0$	$5.979 \times 10^{13}$ (rad/s)	$7.969 \times 10^{13}$ (rad/s)
$\Gamma_1$	$1.07 \times 10^{15}$ (rad/s)	$7 \times 10^{14}$ (rad/s)
$\Gamma_2$	$1.69 \times 10^{15}$ (rad/s)	$9 \times 10^{14}$ (rad/s)
$f_0$	1.039	1.029
$f_1$	0.1108	0.06
$f_2$	0.3202	0.165
$\omega_{0,1}$	$4.428 \times 10^{15}$ (rad/s)	$6.538 \times 10^{15}$ (rad/s)
$\omega_{0,2}$	$5.746 \times 10^{15}$ (rad/s)	$7.328 \times 10^{15}$ (rad/s)
$\varepsilon_\infty$	5.5	2.83
$\xi_1$	− 0.8	− 0.3
$\xi_2$	− 9	− 9

The local modified permittivity is thus a function of position as well as frequency:

$$\varepsilon'_r(r, \omega) = \varepsilon_r(\infty) + \omega'^2_p(r) \sum_{m=0}^M \frac{f_m}{\omega'^2_{0,m}(r) - \omega^2 - j\omega\Gamma_m} \quad (\text{S3})$$

where  $\omega'_p$  and  $\omega'_{0,m}$  are the modified local plasma and inter-band transition frequencies, respectively.  $\omega'_p$  is calculated using the local free electron density of the deformed geometry, whereas  $\omega'_{0,m} = \omega_{0,m} + \delta E_{0,m}/\hbar$ . The net permittivity is a weighted average of the local permittivity using the volume fraction,  $v_f(r)$ , as the weighting factor, where  $r$  represents the position:

$$\varepsilon_{net}(\omega) = \frac{1}{V'} \int_{vol} \varepsilon'_r(r, \omega) dV' \quad (\text{S4})$$

where  $V'$  is the volume of the deformed particle. The above integral is solved numerically by approximating it as a sum over finite number of volume elements:  $\varepsilon_{net}(\omega) = \sum_{r=1}^N v_f(r) \varepsilon'_r(r, \omega)$ , where  $\sum_{r=1}^N v_f(r) = 1$ .

To demonstrate the validity of Equation S4, we compare the optical response of a gold nanosphere obtained using Equation S3 to that obtained using Equation S4. Due to spherical symmetry, the local permittivity of the nanosphere is almost constant within a thin shell. A gold nanosphere can thus be represented by concentric shells of permittivity  $\varepsilon_n(\omega)$ , where  $n$  represents the shell number, as shown in the inset of Figure S1d. The real and imaginary parts of the *net* dielectric constant (Eq. S4) are shown in Figure S1a and b, and the local dielectric constants of each shell (Eq. S3) are shown in Figure S1c and d. It can be seen that the inner shells undergo larger dilation than the outer shells, resulting in a greater modification of the dielectric constant; however, because of their lower volume fraction, the inner shells make a limited contribution to the net dielectric constant.

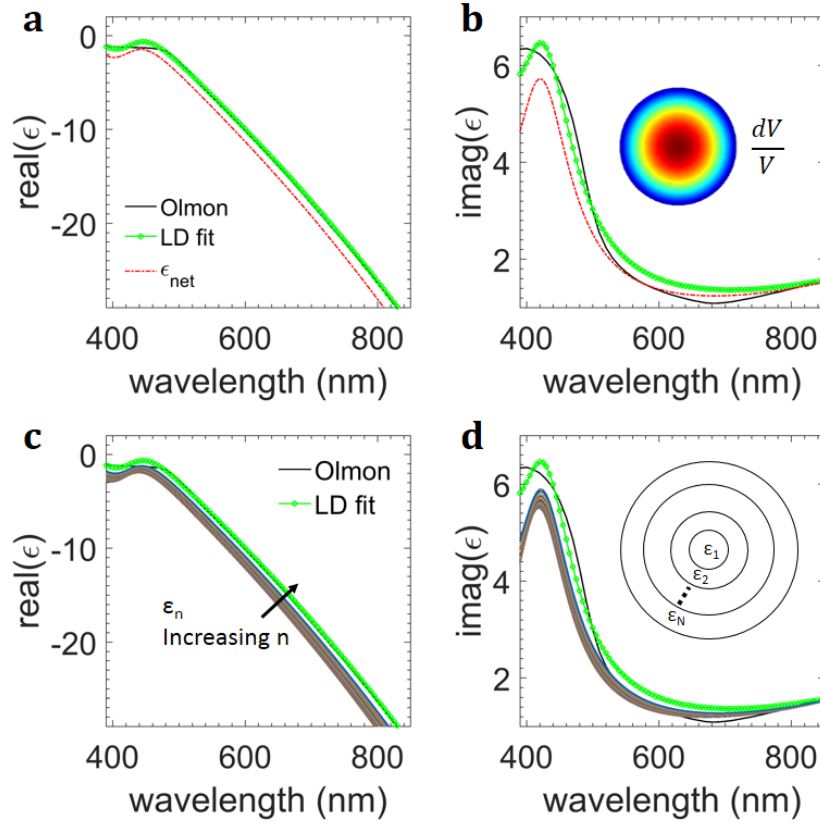


Figure S1. Real and imaginary parts of the dielectric constant of gold obtained using a Lorentz-Drude (LD) fit to the experimental data of Olmon *et al.*, Ref. [1]. (a, b) show the net permittivity of a gold sphere whose radius has been reduced by 1-nm, calculated using Equation S4. The inset in (b) shows the corresponding local volume change. (c, d) show the permittivity of N concentric shells calculated using Equation S3. The inset in (d) illustrates the concentric shells forming the nanosphere.

The optical response of the nanosphere calculated using the two methods discussed above is shown in Figure S2. It can be seen that the extinction cross-sections obtained using the net permittivity are almost identical to the cross-sections that are calculated based on the permittivity of concentric thin shells. Figure S2 also shows the electric field intensities  $|E/E_0|^2$  (log scale) within the solid sphere (b) and shells (c) at a wavelength of 510 nm, where  $E_0$  is the incident electric field. The intensity profiles and electric field enhancement calculated using the two methods are in good agreement.

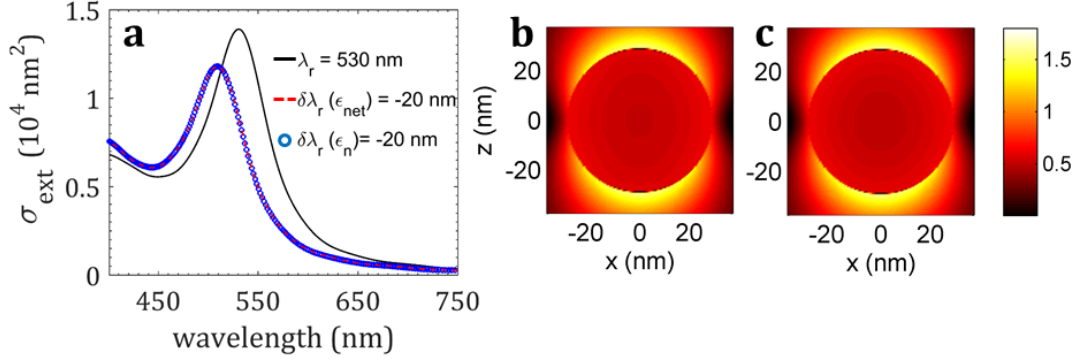


Figure S2. (a) Extinction cross-section of a 60-nm gold nanosphere. The solid black line shows the result for a non-deformed nanosphere, and the dashed red and blue circles show the response due to 1 nm compression of the radius of the sphere, calculated using the net and local permittivities respectively, respectively. (b, c) Electric field intensity  $|E/E_0|^2$  (log scale) using net (b) and local permittivities (c) at a wavelength of 510 nm.

We also investigated the optical response of gold nanoshells using the two methods and found the results to be in good agreement, as shown in Figure S3. The permittivity of the remaining geometries studied in this work were therefore modeled using Equation S4.

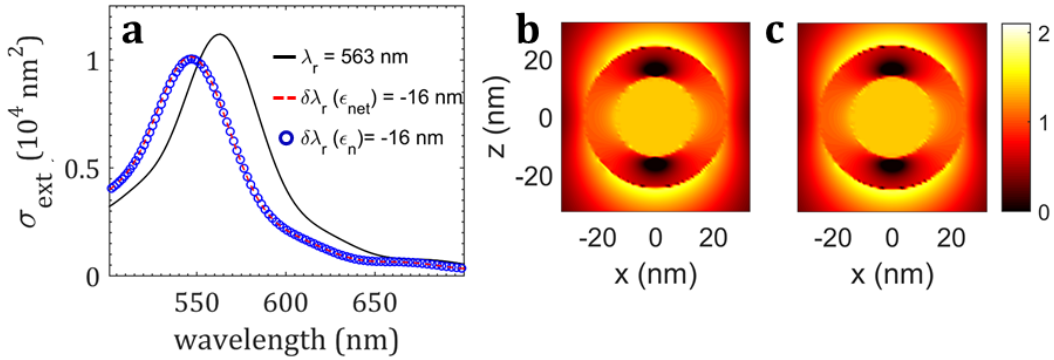


Figure S3. (a) Extinction cross-section of a gold nanoshell with inner radius of 15-nm and outer radius of 25-nm. The solid black line shows the result for a non-deformed hollow sphere, the dashed red and blue circles show the extinction of the deformed hollow sphere corresponding to the fundamental breathing mode, calculated using the net and local permittivities, respectively. (b, c) Electric field intensity  $|E/E_0|^2$  (log scale) using net (b) and local permittivities (c) at a wavelength of 545 nm.

## **TRANSFER OF DEFORMED GEOMETRIES BETWEEN CALCULATIONS**

Extinction cross-sections of the particles are calculated using Lumerical FDTD Solutions<sup>5</sup>. The deformed geometry is transferred from COMSOL to Lumerical for calculations of optical properties. The transformation procedure depends upon the geometry. Simple geometries such as the sphere and shell can easily be reproduced in Lumerical by adjusting the radius in accordance with the results of the COMSOL simulations. Rods and cubes, however, require further processing to model the deformed geometry on the rectangular mesh of Lumerical.

In the case of rods, a cross-section of the rod in a 2D plane through the center of the rod is exported from COMSOL into Matlab, and is then rotated 180 degrees to generate the surface of revolution representing the surface of the deformed rod. A rectangular mesh is then created, the grid points inside the rod's surface are given a value of unity, and the remaining points are set to zero. The resulting matrix is then saved as a text file that can be imported into Lumerical.

For nanocubes, we exported the surface of one face of the deformed cube into Matlab. Using the `scatteredInterpolant` function of Matlab and then querying that function at rectangular grid allowed for the transformation of the deformed surface from a tetrahedral to a rectangular mesh. The deformation of the other five faces of the cube were then calculated by using the information provided by one face. As in the case of the rod, a text file is created containing ones and zeros to be imported in Lumerical.

## LINEARITY AND INTERPOLATION

We calculated the change in the optical spectrum of a 60-nm gold sphere for a series of changes in diameter, from 0.25 nm to 1.0 nm. As shown in Figure S4, the shift in the plasmon resonance frequency is linear with respect to the change in the diameter of the sphere.

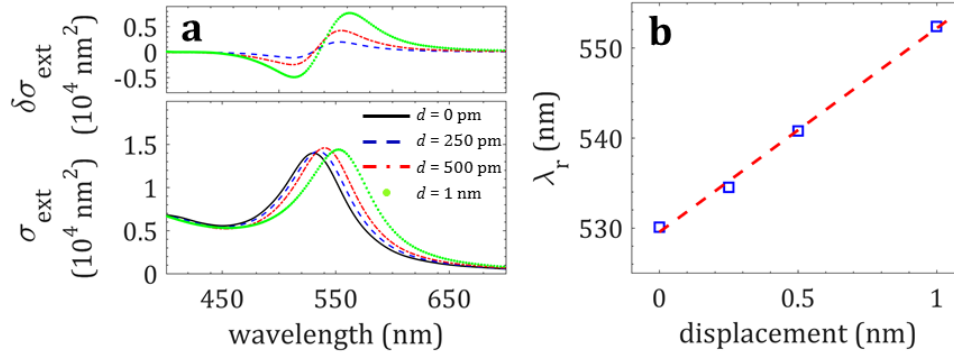


Figure S4. Calculation results for a 60-nm gold sphere showing plasmon resonance shift for varying phonon vibrational amplitudes. (a) Changes in extinction cross-section for vibrational amplitude  $d$  of 1-nm (green dots), 0.5-nm (dashed-dot red), 0.25-nm (dashed blue) and 0-nm (solid black). (b) Plasmon resonance wavelength as a function of deformation amplitude. Blue squares represent the calculated values and dashed red line is a linear fit.

The calculated optical response can thus be linearly interpolated to find the plasmon shift corresponding to arbitrarily small deformations. Consider two numerically calculated spectra  $A(\lambda)$  and  $B(\lambda)$  corresponding to vibration amplitudes of 0 nm and 1 nm, respectively, assuming the plasmon peak of  $B(\lambda)$  is shifted by  $\Delta\lambda^{1nm}$  compared to  $A(\lambda)$ . Suppose we would like to find the interpolated spectrum  $C(\lambda)$  for a deformation of  $d$  ( $d < 1\text{nm}$ ). Using  $\alpha = d/1\text{nm}$  and  $\beta = 1 - \alpha$ , we can write  $C(\lambda) = [\beta A(\lambda - \alpha \Delta\lambda^{1nm}) + \alpha B(\lambda + \beta \Delta\lambda^{1nm})]$ . Interpolated results for deformations of 125 pm and 250 pm are shown in Figure S5.

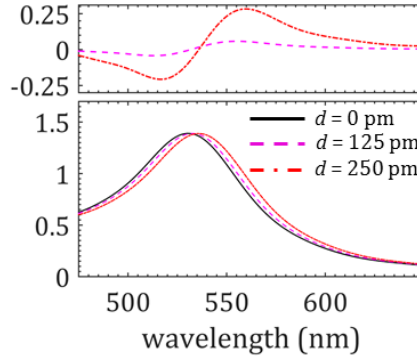


Figure S5. Interpolated results for a 60-nm gold sphere showing extinction spectra for deformation of 125-pm (dashed magenta) and 250-pm (dashed-dot red). The interpolation is carried out using the calculated results corresponding to deformation amplitude of 1-nm (not shown here) and 0 pm (solid black) and assuming a linear relation between plasmon shift and deformation amplitude.

We performed similar calculations for deformations of a gold nanorod. As shown in Figure S6, the shift in plasmon frequency is again linear with respect to the amplitude of deformation. We thus expect that the interpolation of optical signal to smaller amplitudes will work for arbitrary nanoparticle geometry.

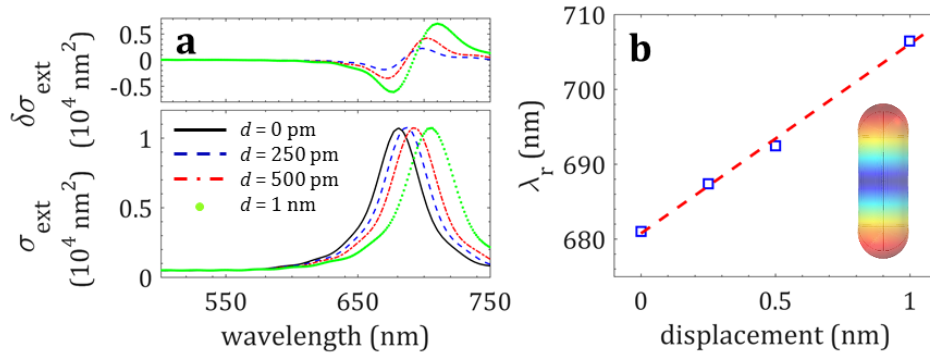


Figure S6. Calculation results for a 61-nm long and 22-nm wide gold nanorod. (a) Changes in extinction cross-section for vibrational amplitude  $d$  of 1 nm (green dots), 0.5 nm (dashed-dot red), 0.25 nm (dashed blue) and 0 nm (solid black). (b) Plasmon resonance wavelength as a function of deformation amplitude. Blue squares represent the calculated values and dashed red line is a linear fit.

## EXTINCTION CROSS-SECTIONS AND VARIOUS COUPLING MECHANISMS

In the following, we present the calculated extinction cross-sections of all the geometries studied in this work as the nanoparticles expand. We separately calculate contributions from shape, electron density (ED), and deformation potential (DP) to the overall shift in the plasmon resonance.

Figure S7a shows results for a 60-nm gold nanosphere in response to 1 nm expansion, corresponding to the fundamental breathing mode of the sphere. It is seen that deformation potential is the dominant effect, because of the proximity of the inter-band transition frequencies to the plasmon resonance of the sphere. Results for the higher-order breathing mode are shown in Figure S7b. In this case, all contributions are small. Similar results for a 60-nm silver sphere are shown in Figure S8.

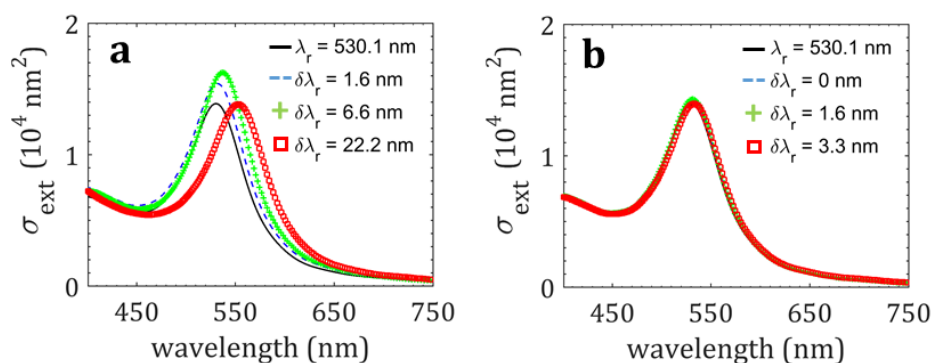


Figure S7. Change in extinction cross-section of a 60-nm gold nanosphere corresponding to the (a) fundamental and (b) higher-order breathing modes as the particle undergoes expansion. Undeformed (solid black line); shape effect only (dashed blue line); shape and electron density effects only (green plus signs); shape, electron density and deformation potential effects (red squares).

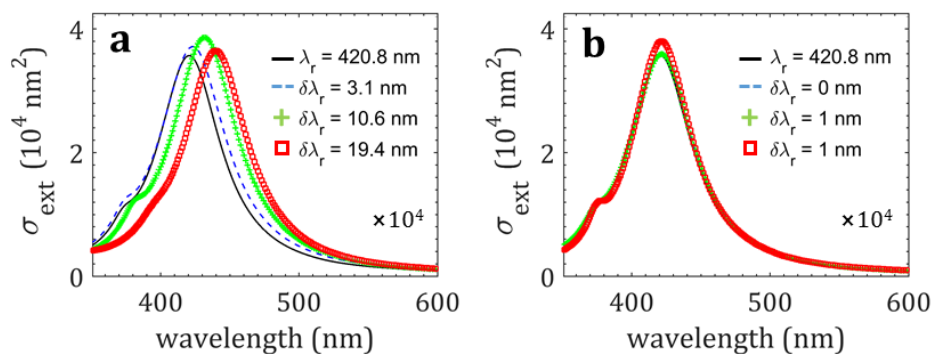


Figure S8. Change in extinction cross-section of a 60-nm silver nanosphere corresponding to the (a) fundamental and (b) higher-order breathing modes as the particle undergoes expansion. Un-deformed (solid black line); shape effect only (dashed blue line); shape and electron density effects only (green plus signs); shape, electron density and deformation potential effects (red squares).

Figures S9 and S10 show the results for gold nanorods due to extensional modes (left panels) and breathing modes (right panels). The results are in good agreement with the experimental transient absorption result for single gold nanorods in water.<sup>6</sup>

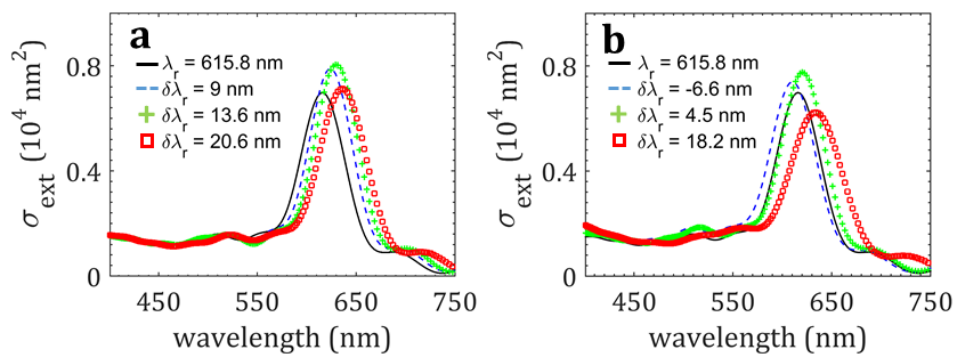


Figure S9. Change in extinction cross-section of a 55-nm long and 26-nm wide gold nanorod corresponding to the (a) extensional and (b) breathing modes as the particle undergoes expansion. Un-deformed (solid black line); shape effect only (dashed blue line); shape and electron density effects only (green plus signs); shape, electron density and deformation potential effects (red squares).

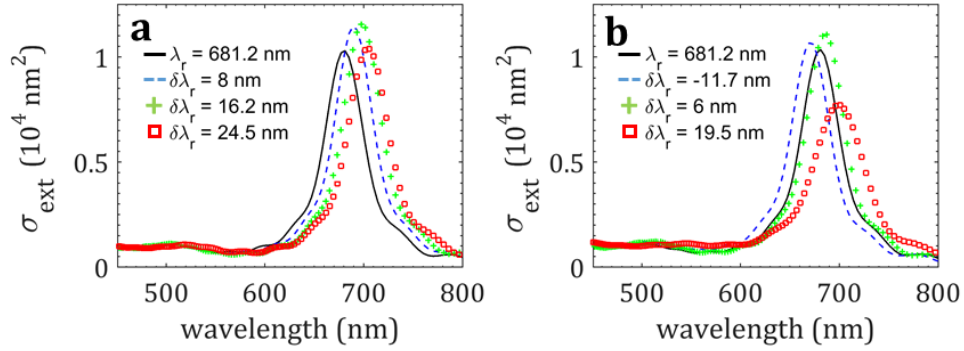


Figure S10. Change in extinction cross-section of a 61-nm long and 22-nm wide gold nanorod corresponding to the (a) extensional and (b) breathing modes as the particle undergoes expansion. Un-deformed (solid black line); shape effect only (dashed blue line); shape and electron density effects only (green plus signs); shape, electron density and deformation potential effects (red squares).

Figure S11 shows the results for silver nanorods. In this case, the plasmon shift due to the breathing mode is significantly lower, because the large spectral separation between inter-band transition energies and the plasmon resonance frequency means that DP effects are negligible. Vibrational modes also couple to the transverse vibrational mode of the silver nanorod. We observe an order of magnitude weaker coupling of the extensional phonon mode to transverse plasmon mode as compared to its coupling to the longitudinal plasmon mode. The breathing mode of the rod couples somewhat to the transverse plasmon mode, with about 1/3 of the coupling strength as compared to its coupling to the longitudinal plasmon mode.

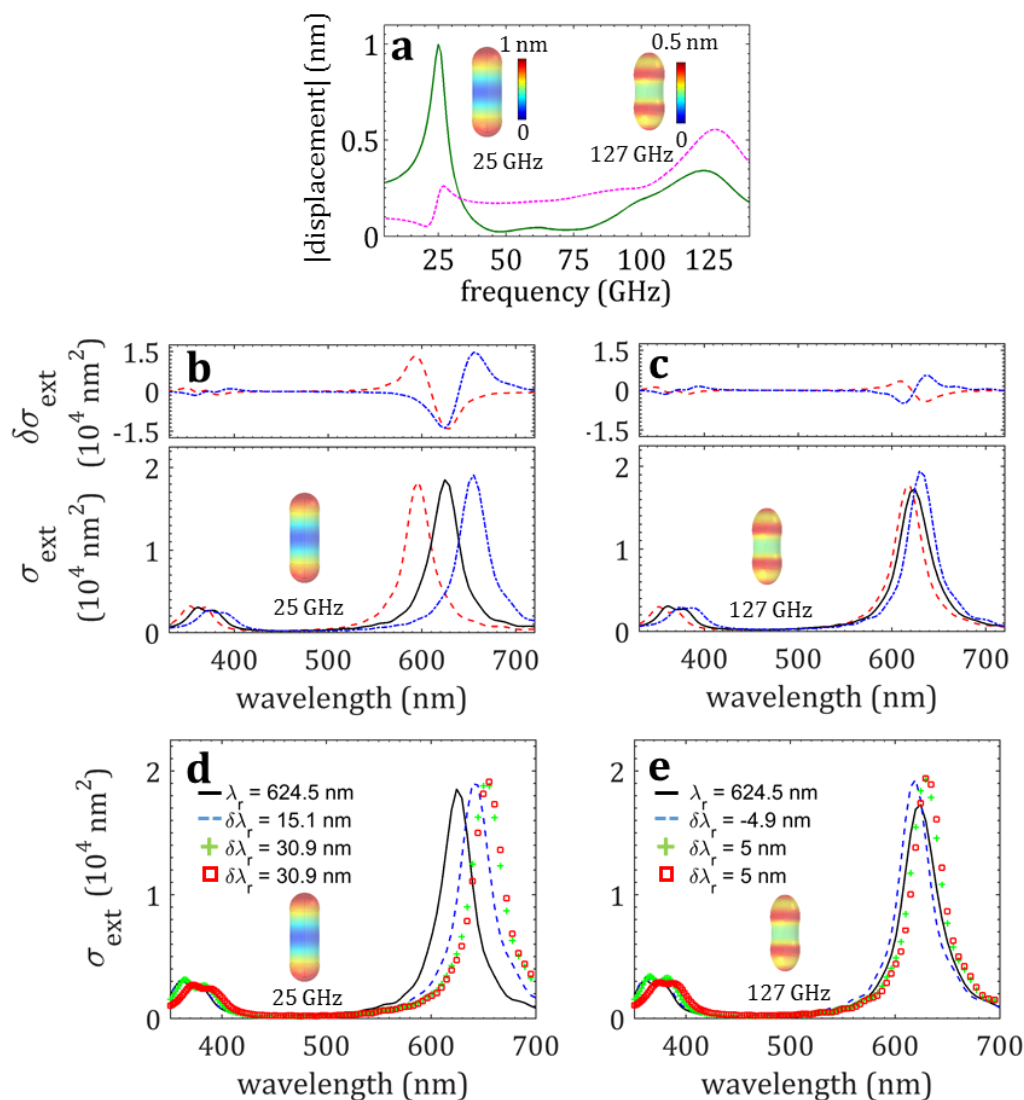


Figure S11. (a) Displacement of the end (solid green) and of the mid-point (dashed magenta) of a 61-nm long and 22-nm wide silver nanorod as a function of frequency. (b, c) Change in extinction cross-section corresponding to the extensional (b) and breathing (c) modes. (d, e) Contribution from the various effects to the overall shift in plasmon resonance in response to expansion of the particle: undeformed (solid black line); shape effect only (dashed blue line); shape and electron density effects only (green plus signs); shape, electron density and deformation potential effects (red squares).

Results for a 40 nm gold nanoshell are shown in Figure S12. For the fundamental breathing mode, the inner and outer surfaces are displaced in phase outwardly, causing an overall expansion of the particle. For the higher-order breathing mode, the inner and outer surfaces move 180 degrees out of phase. Figure S12b shows the results when the inner surface is displaced

outwardly while the outer surface is displaced inwardly by equal amount, resulting in an overall compression of the nanoshell, as shown in the inset by the negative local volume change. The shape change and changes in permittivity produce plasmon shifts in opposite directions, making this mode difficult to detect in TA experiments.

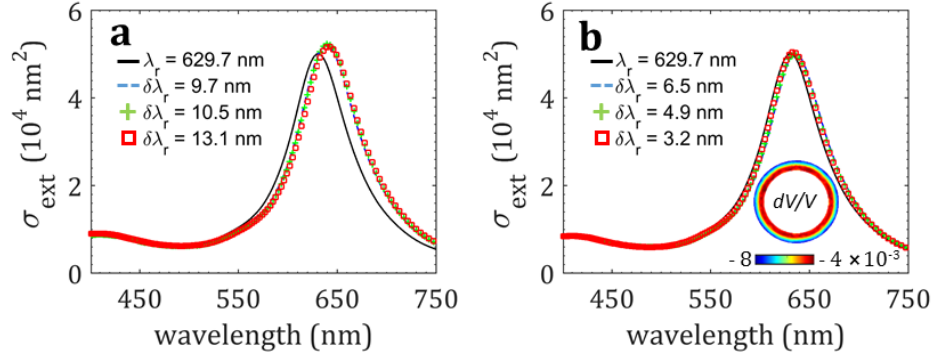


Figure S12. (a, b) Change in extinction cross-section for a gold nanoshell with  $R_{\text{out}} = 40\text{-nm}$  and  $R_{\text{in}} = 30\text{-nm}$  corresponding to the fundamental (a) and higher-order (b) breathing modes. Undeformed (solid black line); shape effect only (dashed blue line); shape and electron density effects only (green plus signs); shape, electron density and deformation potential effects (red squares).

Results for a smaller nanoshell with outer radius of 25 nm and shell thickness of 10 nm are shown in Figure S13. Deformation potential plays a significant role in this case, as can be expected for a plasmon resonance at a shorter wavelength. The higher-order breathing mode results in both compression and expansion at different radial positions, as seen in the inset of Figure S13b. The net effect is in-phase modulation of the plasmon resonance by all three coupling mechanisms, making this mode easily detectable in TA measurements. This is in good agreement with experimental results.

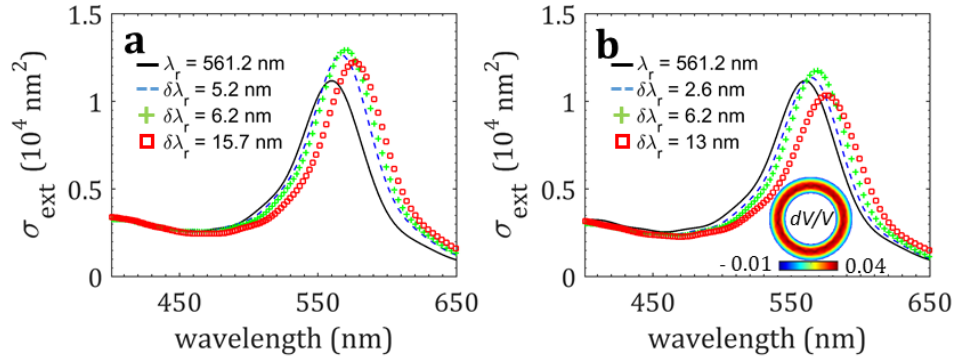


Figure S13. (a, b) Change in extinction cross-section of a gold nanoshell with  $R_{\text{out}} = 25\text{-nm}$  and  $R_{\text{in}} = 15\text{-nm}$  corresponding to the fundamental (a) and higher-order (b) breathing modes. Undeformed (solid black line); shape effect only (dashed blue line); shape and electron density effects only (green plus signs); shape, electron density and deformation potential effects (red squares).

The optical response of silver nanocubes to phonon vibrations is presented in Figures S14 and S15. Deformation potential is the least significant coupling mechanism, because of the large spectral gap between the inter-band transition and plasmon frequencies. The higher-order breathing mode of the smaller nanocube (Fig. S14, 35 nm edge length) results in almost no plasmon shift, because shape and permittivity effects cancel almost completely.

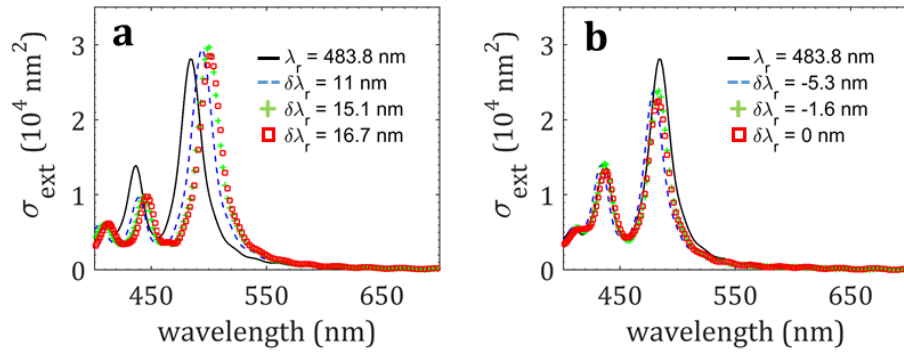


Figure S14. Change in extinction cross-section of a 35-nm silver nanocube corresponding to the fundamental (a) and higher-order (b) breathing modes as the particle undergoes expansion. Undeformed (solid black line); shape effect only (dashed blue line); shape and electron density effects only (green plus signs); shape, electron density and deformation potential effects (red squares).

The larger nanocube (Fig. S15, 85 nm edge length) shows very different extinction spectra, with large scattering for the larger particle size. Fundamental and higher-order breathing modes produce comparable plasmons shifts, but 180 degrees out of phase with one another. These results are also in good agreement with experimental findings.

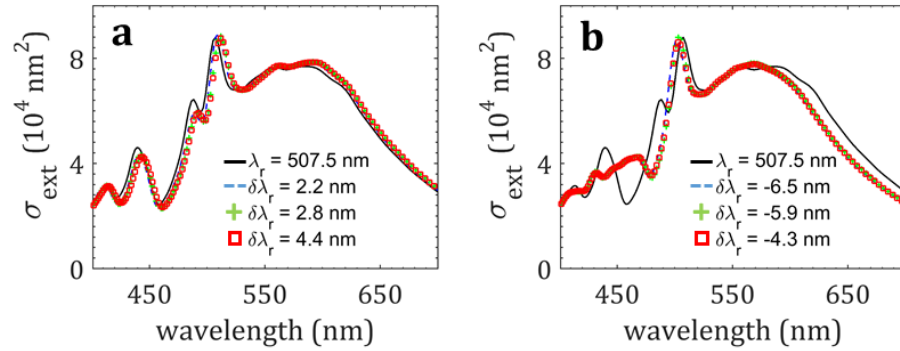


Figure S15. Change in extinction cross-section of a 85-nm silver nanocube corresponding to the fundamental (a) and higher-order (b) breathing modes as the particle undergoes expansion. Undeformed (solid black line); shape effect only (dashed blue line); shape and electron density effects only (green plus signs); shape, electron density and deformation potential effects (red squares).

## REFERENCES

1. Olmon, R. L.; Slovick, B.; Johnson, T. W.; Shelton, D.; Oh, S.-H.; Boreman, G. D.; Raschke, M. B. Optical Dielectric Function of Gold. *Phys. Rev. B* **2012**, *86*, 235147.
2. Yang, H. U.; D'Archangel, J.; Sundheimer, M. L.; Tucker, E.; Boreman, G. D.; Raschke, M. B. Optical Dielectric Function of Silver. *Phys. Rev. B* **2015**, *91*, 235137.
3. Szczepanek, P.; Glosser, R. Piezo-Optical Constants of Gold. *Solid State Commun.* **1974**, *15*, 1425-1429.
4. Tups, H.; Otto, A.; Syassen, K. Pressure Dependence of the *D*-Band to Fermi-Level Excitation Threshold in Silver. *Physical Review B* **1984**, *29*, 5458-5461.

5. Lee, A.; Andrade, G. F. S.; Ahmed, A.; Souza, M. L.; Coombs, N.; Tumarkin, E.; Liu, K.; Gordon, R.; Brolo, A. G.; Kumacheva, E. Probing Dynamic Generation of Hot-Spots in Self-Assembled Chains of Gold Nanorods by Surface-Enhanced Raman Scattering. *J. Am. Chem. Soc.* **2011**, *133*, 7563-7570.
6. Yu, K.; Zijlstra, P.; Sader, J. E.; Xu, Q.-H.; Orrit, M. Damping of Acoustic Vibrations of Immobilized Single Gold Nanorods in Different Environments. *Nano Lett.* **2013**, *13*, 2710-2716.